

EVIDENCE OF A MINORITY MONOCLINIC $\text{LaNiO}_{2.5}$ PHASE IN LANTHANUM NICKELATE THIN FILMS

L. López-Conesa¹, J.M. Rebled^{1,2,4}, D. Pesquera², N. Dix², F. Sánchez², G. Herranz², J. Fontcuberta², C. Magén^{5,6}, M.J. Casanove³, S. Estradé¹ and F. Peiró¹

1. Laboratory of Electron Nanoscopy (LENS-MIND-IN²UB), Institute of Nanoscience and Nanotechnology, Electronics Department, University of Barcelona, c/ Martí i Franqués 1. Barcelona 08028. Catalonia. Spain
2. Institut de Ciència de Materials de Barcelona (ICMAB-CSIC), Campus UAB, Bellaterra 08193, Catalonia. Spain
3. Centre d'Élaboration des Matériaux et d'Etudes Structurales (CEMES-CNRS), 29 rue Jeanne Marvig, BP 94347, 31055 Toulouse Cedex 4. France
4. Centres Científics i Tecnològics de la Universitat de Barcelona (CCiT-UB), c/ Lluís Solé i Sabarís s/n, 08028
5. Laboratorio de Microscopías Avanzadas (LMA) - Instituto de Nanociencia de Aragón (INA) and Departamento de Física de la Materia Condensada, Universidad de Zaragoza, 50018 Zaragoza, Spain
6. Fundación ARAID, 50018 Zaragoza, Spain

Abstract

LaNiO_3 (LNO) thin films of 14 nm and 35 nm thicknesses grown epitaxially on LaAlO_3 (LAO) and $(\text{LaAlO}_3)_{0.3}(\text{Sr}_2\text{TaAlO}_6)_{0.7}$ (LSAT) substrates are studied by High Resolution Transmission Electron Microscopy (HRTEM) and (High Angle Annular Dark Field (HAADF) imaging. The strain state of the films is studied by Geometric Phase Analysis (GPA). Results show the successful in-plane adaptation of the films to the substrates, both in the compressive (LAO) and tensile (LSAT) cases. Through the systematic analysis of HRTEM superstructure contrast modulation along different crystal orientations, localized regions of the monoclinic $\text{LaNiO}_{2.5}$ phase are detected in the 35 nm films.

1. Introduction

The series of rare earth nickelates (RENiO_3) presents a very rich phenomenology among the transition metal oxides due to the interplay of charge, orbital, spin and crystal lattice degrees of freedom. Even more so when considering epitaxial thin films for which additional new phases, different from the bulk ones, may appear. The case of LaNiO_3 (LNO) is of particular interest, since it is one of the few oxides for which resistivity levels below $100 \mu\Omega\cdot\text{cm}$ at room temperature have been reported [Xu1993,Zhu2013], so it could be used as a highly conducting oxide electrode. In addition, it is the only member of the RENiO_3 series that keeps its metallic character for all temperatures, with no metal-insulator (MI) transition, except for ultrathin films of less than eight unit cells [Scherwitzl2009].

These capabilities of LNO have given rise to an increasing number of attempts at obtaining nanostructures with new and interesting properties through interface effects such as strain engineering. The combinations of LNO and different complex oxides in multilayered systems aim at obtaining artificial high T_c superconductors, for example [Poltavets2010]. However, in most of the reported systems, LNO films are either considered to be fully elastically strained or the strain relaxation is explained in terms of crystal symmetry modifications keeping the stoichiometry in the film constant. In this work, we report on LNO thin films with two different thicknesses (14 nm and 35 nm), grown on (001)-oriented substrates exerting compressive [LaAlO_3 , (LAO)] or tensile stress [$(\text{LaAlO}_3)_{0.3}(\text{Sr}_2\text{TaAlO}_6)_{0.7}$ (LSAT)] on the films. The strain state of the films is assessed by Geometric Phase Analysis (GPA) of High Angle Annular Dark Field (HAADF) transmission electron microscopy (TEM) images. Beyond the long-range

symmetry effects of substrate-induced strain on the films already reported in [Weber2016], or the presence of local planar defects of the Ruddlesden-Popper type [Coll2016], in this work we address the role of possible local, short-range, non-stoichiometry in LNO films through the analysis of superstructure contrast modulation in high-resolution TEM (HRTEM) images.

2. Methods

A series of films were grown by pulsed laser deposition on top of LAO (-1.1 % lattice mismatch) and LSAT (+0.7 % lattice mismatch) substrates using a KrF excimer laser ($\lambda = 248$ nm). The laser beam was focused on a stoichiometric ceramic LaNiO_3 target with a fluence of around $1.5 \text{ J}\cdot\text{cm}^{-2}$ and at a repetition rate of 5 Hz. Deposition was performed at an oxygen pressure of 0.15 mbar and keeping the substrate at a temperature of 700 °C. The number of laser pulses was varied to obtain films with nominal thicknesses of 14 nm and 35 nm, according to previous growth-rate calibrations. HRTEM images were obtained in a JEOL 2010F and a JEOL 2100. HAADF images were obtained in a probe-corrected FEI Titan Low 60-300. Atomic resolution images were analyzed using Geometric Phase Analysis (GPA) [Snoeck1998] in order to characterize the strain states of the films.

3. Results and discussion

Figures 1 and 2 show HAADF images of the 14 nm- and 35 nm-thick LNO films, respectively, grown on LAO and LSAT. They present good crystalline quality. Cube-on-cube $[001]\text{LNO}(010)//[001]\text{substrate}(010)$ epitaxy relationship and atomic-sharp interfaces are observed. The corresponding Fast-Fourier Transforms FFTs of the images, obtained from the film region, show the epitaxial growth of the films on both

substrates, with no detectable crystal symmetry change between the compressive and tensile cases for the strained LNO films.

Geometric Phase Analysis was used to generate strain tensor maps for the in-plane (ϵ_{xx}) and out-of-plane (ϵ_{yy}) components, using the substrate region as a reference. Strain maps for the 14 nm thick and the 35 nm thick LNO films are shown in figures 1 and 2 respectively, superimposed to the experimental HAADF images. From the GPA results, it can be seen that films grow fully adapted to the substrate in the in-plane direction for the first nanometers. The ϵ_{yy} component was further analysed, and taking into account the difference between the lattice parameters of each substrate and the bulk LNO lattice parameter, it was found that all films present out of plane parameters that lie close to the LNO lattice parameter bulk value ($a = 3.838 \text{ \AA}$). The difference is of 0.7% for LNO on LAO and 0.1% for LNO on LSAT. The estimated error in the GPA maps is of 0.3 %.

It is worth noticing the presence of planar defects in all the films after the first 2 - 3 nm of growth, highlighted in figures 1 and 2 by dashed white lines. The detailed characterization of these defects can be found elsewhere [Coll2016].

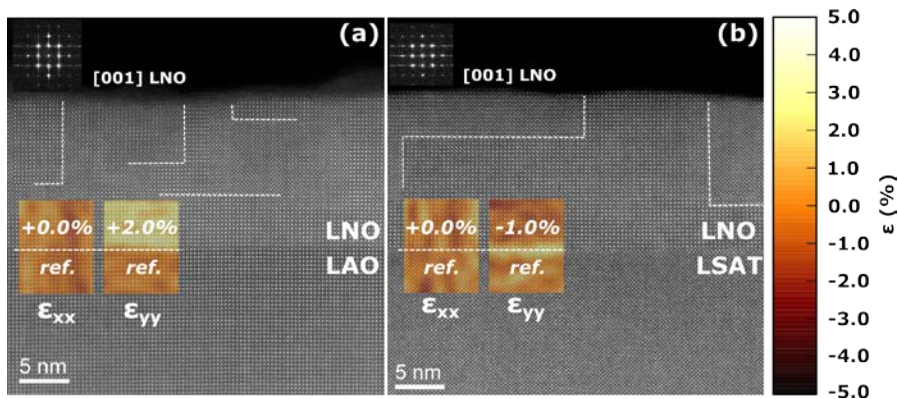


Fig. 1. HAADF images of 14 nm thick LNO films grown on LAO (a) and LSAT (b). Insets show the corresponding FFTs obtained from the film region in each case. All the LNO films present the same structure, with an elastically deformed unit cell due to the substrate-induced strain. Superimposed in color, GPA maps for the in-plane (ϵ_{xx}) and out-of-plane (ϵ_{yy}) components of the strain tensor, using the substrate region as a reference. In-plane components show a fully adapted film.

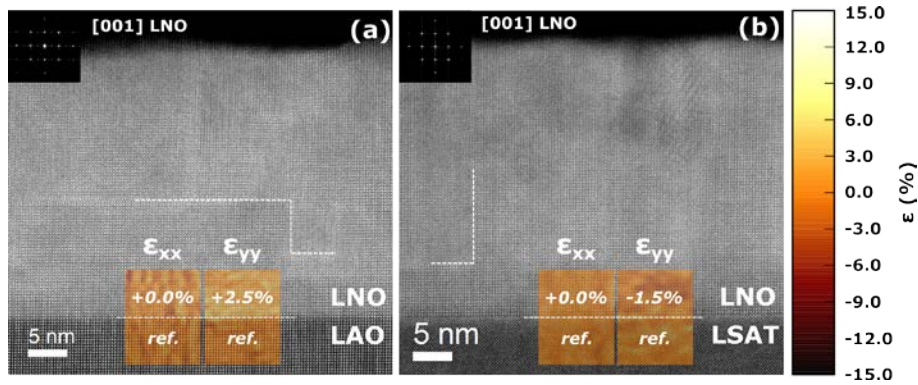


Fig. 2. HAADF images of the 35 nm thick LNO films grown on LAO (a) and LSAT (b). Insets show the corresponding FFTs obtained from the film region in each case. All the LNO films present the same structure, with an elastically deformed unit cell due to the substrate-induced strain. Superimposed in color scale, GPA maps for the in-plane (ϵ_{xx}) and out-of-plane (ϵ_{yy}) components of the strain tensor, using the substrate region as a reference. In-plane components show a fully adapted film.

Upon further inspection, some localized regions are detected in the 35 nm films presenting a superstructure contrast modulation. This is not the case for the 14 nm films. Figure 3 shows an HRTEM image of the 35 nm LNO film on LAO observed along the [100] zone axis with a superstructure modulation oriented perpendicular to the substrate-film interface, doubling the d_{010} spacing. In the following, we aim our analysis at understanding the origin of this feature.

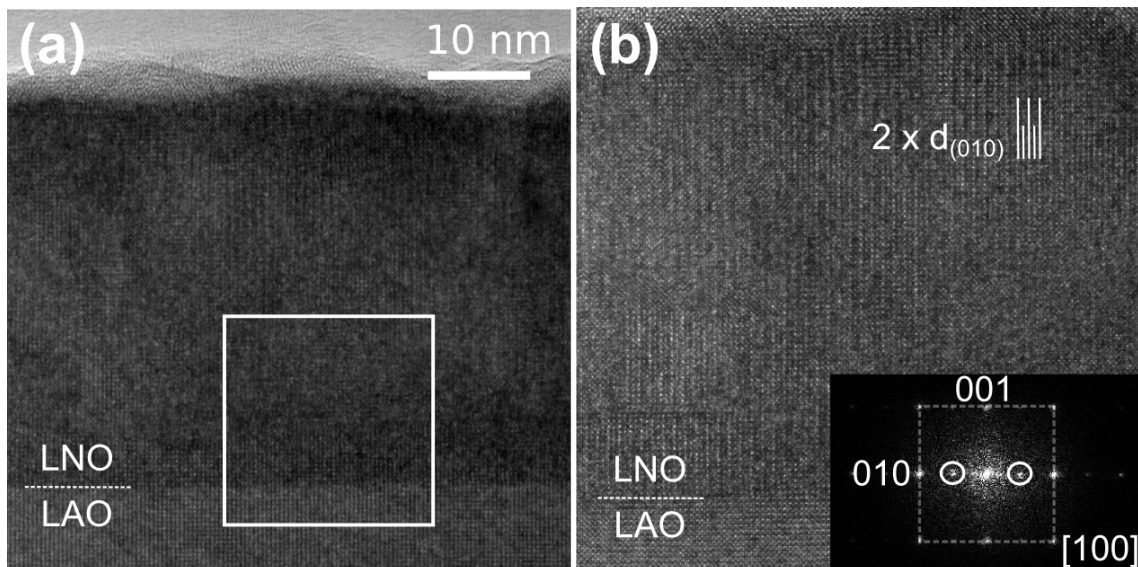


Fig. 3. a) HRTEM image of the 35 nm LNO film grown on LAO taken along the [100] zone axis. b) Close-up view and FFT from the highlighted area. A superstructure modulation is observed in this particular region of the film, consisting in a doubling of the periodicity of the unit cell in the in-plane [010] direction. This can be seen as the $1/2 \times (010)$ spot in the FFT and in real space as the doubling of the d_{010} spacing, as indicated.

Superstructure modulation in complex oxides with a perovskite, or a related, structure is rather common. The extremely large flexibility of the perovskite unit cell, which allows it to accommodate cations of very different sizes, results in a broad landscape of possible superstructures for distorted perovskites. The distortion of the coordination polyhedra might consist in just a collective rotation pattern of the BO_6 octahedra [Woodward2005] or in the formation of different coordination environments for all or some of the cations, if vacancies are introduced. The relaxation of the cation positions around a structural defect, such as an oxygen vacancy, results in the rearrangement of the remaining oxygen atoms to create new coordination polyhedra [Stolen2005,Stolen2006]. In the well known series of defective perovskites described by the formula $\text{A}_n\text{B}_n\text{O}_{3n-1}$, there is a variety of local minima for the energy corresponding to the rearrangement of the structure when oxygen atoms are taken away. Given the inherent thermodynamic instability of the Ni^{3+} state, let us now consider the $n = 2$ member of the series. This gives us the oxygen deficient $\text{LaNiO}_{2.5}$ phase.

Investigations on the structure of the $\text{LaNiO}_{2.5}$ sub-stoichiometric phase go back to the 1980s when an XRD pattern was first reported by Crespin *et al.* [Crespin1983] and indexed as a monoclinic perovskite superstructure with cell parameters $\sqrt{2}a_o, \sqrt{2}a_o, 2a_o$, being a_o the cell parameter of the ideal cubic perovskite. Although the structure could not be solved, a model based on the brownmillerite structure was proposed. Brownmillerite is a perovskite superstructure in which the B cation adopts both tetrahedral and octahedral coordination due to the ordering of the oxygen vacancies. However, given that a tetrahedral environment is particularly unfavorable in the case of Ni, tetragonal structures were proposed by Vidgasayar and Rao [Kinyanjui2014], in which the ordering of oxygen vacancies occurs in the [110]

direction, forming chains of NiO₆ octahedra and NiO₄ square planes aligned along the *c* axis. Based on electron diffraction experiments, González-Calbet *et al.* [GonCal1989] adopted the octahedral-square planes description but in the framework of a monoclinic cell with $\sqrt{2}a_o, \sqrt{2}a_o, 2a_o$ cell parameters. Later, Moriga *et al.* [Moriga1994] determined the correct unit cell symmetry from XRD data, which was found to be monoclinic but with a relationship to the ideal perovskite of the form $2a_o, 2a_o, 2a_o$. Given that the finer structural details are determined by the arrangements of oxygen atoms, which are weak scatterers for X-rays, the final refinement of the structure including the polyhedra tilt patterns was reported by Alonso *et al.* [Alonso1997,Alonso1995] from high resolution neutron diffraction experiments. Their results also proved, based on the Brown bond model, that Ni atoms are divalent in both octahedral and square-planar coordination environments.

Figure 4(a) shows the unit cell for the oxygen deficient LaNiO_{2.5}, including the Ni coordination polyhedra only. The lattice parameters are $a_m = b_m = 7.8 \text{ \AA}$, $c_m = 7.40 \text{ \AA}$ and $\beta = 94^\circ$, where the subindex *m* stands for monoclinic. The shortening of the *c* axis is a result of the missing two apical oxygens in the square planar columns, as shown in Figure 4(b). When these apical oxygen atoms are missing, the equatorial oxygen atoms are drawn closer to the central Ni atom. As a result, the equatorial planes of the adjacent octahedral units are expanded and the apical oxygen atoms are drawn closer to the central Ni atom to compensate for this [Alonso1997].

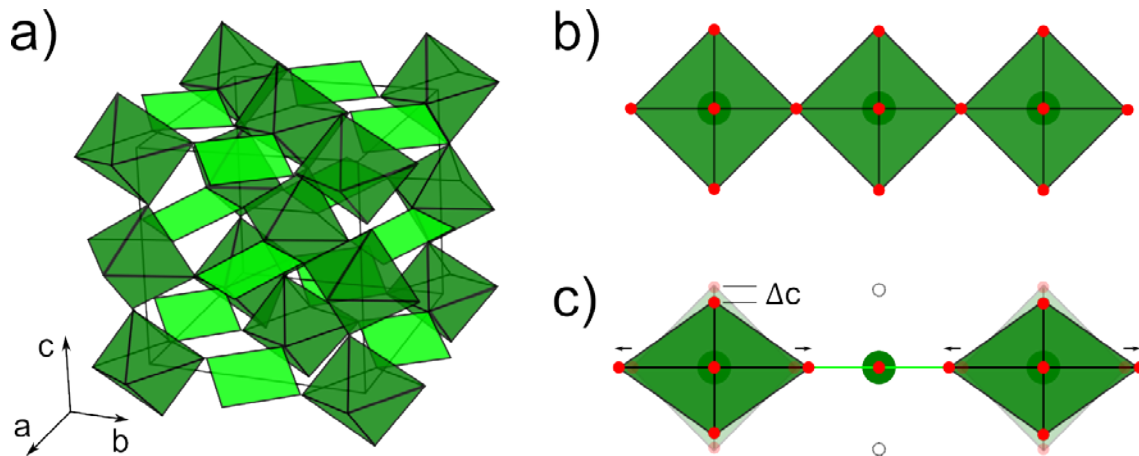


Fig. 4. a) LaNiO_{2.5} monoclinic unit cell showing the two different coordination environments for Ni atoms: octahedra and square planes. Adapted from [Alonso1997]. b) Schematic view of the Ni coordination polyhedra in the ideal perovskite structure. c) Schematic view of the distortion of the Ni coordination polyhedra caused by the missing apical oxygens in every second Ni position along [110]. This distortion is responsible for the shortening of the *c* axis of the monoclinic phase when compared to the ideal perovskite.

Considering the HRTEM image of the 35 nm LNO film grown on LAO shown in Figure 3, taken along the [100] zone axis, and the unit cell of the LaNiO_{2.5} phase, the observed superstructure modulation can be explained as an octahedral tilt arrangement resulting from the missing oxygen atoms. However, images taken along the [100] zone axis can not provide direct imaging of the octahedral and planar coordinated columns, according to the model in figure 4a, since these alternate along the [110] direction.

In order to assess the possible presence of this LaNiO_{2.5} phase let us take into consideration the character of the substrate lattice mismatch. In the case of compressive strain exerted by the LAO substrate, the shorter *c* axis of the monoclinic, oxygen deficient LaNiO_{2.5} is expected to lay in plane. Given the cube-on-cube epitaxial relationship, when preparing a cross-section TEM specimen so that one of the faces of the LAO cubic cell is perpendicular to the electron beam, the *c* axis of the monoclinic phase can end up lying either parallel or perpendicular to the electron beam. The experimental image in figure 5(a), as the one in figure 2, is compatible with the

monoclinic c axis being oriented perpendicular to the electron beam, as illustrated by the model in figure 5c (left). Therefore, by preparing a new TEM specimen from the same sample, cut at 90° from the first one, it is expected to get the monoclinic c axis parallel to the electron beam. In this situation, the chains of NiO_6 octahedra and NiO_4 square planes would be apparent in the image, according to the model shown in figure 5c (right). A new cross section sample was then prepared at 90° and the results are shown in figure 5b. Looking in detail, a region with a contrast modulation consisting in a checkerboard pattern oriented at 45° with respect to the substrate-film interface is visible. This pattern corresponds to the doubling of the (110) interplanar distances, as predicted for the ordering of the oxygen vacancies in $\text{LaNiO}_{2.5}$ viewed along the c axis as in figure 5c (right).

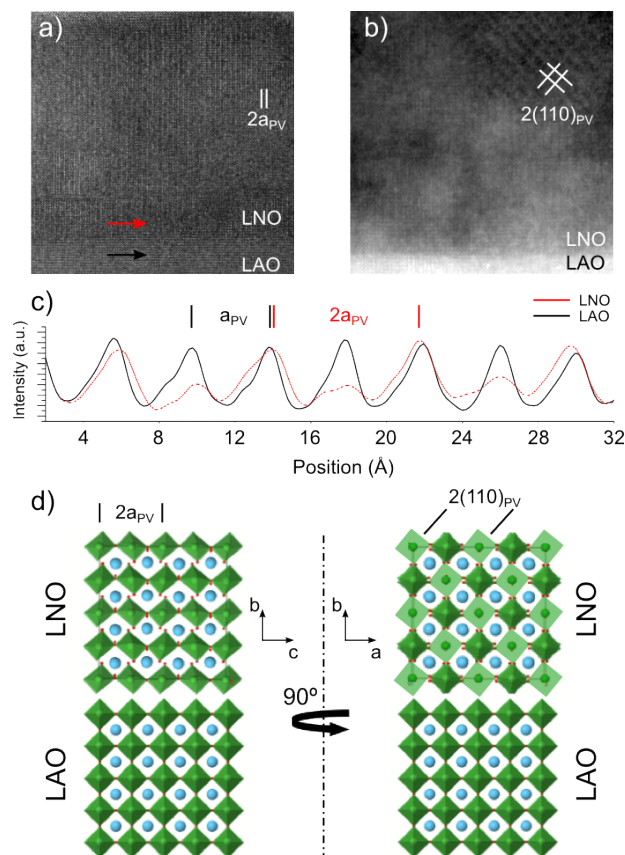


Fig. 5. a,b) Pair of HRTEM images of the 35 nm LNO film on LAO related by a 90° rotation of the sample preparation direction, showing a (faint) superstructure contrast modulation in different

orientations. c) Intensity profiles taken in the substrate (black) and superstructure region in LNO (red), as indicated by arrows in panel a), showing the double periodicity. d) Structural model of the $\text{LaNiO}_{2.5}/\text{LAO}$ interface showing the octahedral tilt pattern of $\text{LaNiO}_{2.5}$, viewed along the **a** axis (left), and the alternating octahedral and planar columns, viewed along the **c** axis (right).

Let us now consider the case of tensile stress. Figure 6(a) shows an HRTEM image of the 35 nm LNO film grown on LSAT. A superstructure modulation doubling the perovskite unit cell is observed in this film too, but oriented parallel to the substrate-film interface. Considering again the $\text{LaNiO}_{2.5}$ phase, this can be understood in terms of the epitaxial strain exerted by the substrate. If the compressive LAO favoured the in-plane orientation of the monoclinic *c* axis, the tensile LSAT favours its out-of-plane orientation. In this situation, irrespective of the face of the cube of the LSAT substrate chosen to be oriented parallel to the electron beam in the cross-section TEM specimen, the ordered columns with oxygen vacancies will not be directly visible. Again, the observed superstructure corresponds to the octahedral tilt pattern, as depicted in the model in Figure 6c (right), where the structural model with the coordination polyhedra is shown. By rotating the structure 45° in-plane so that the (110) planes, in which the ordering occurs, are visible, a new superstructure modulation is expected to be seen, perpendicular to the substrate-film interface, coexisting with the parallel one, which corresponds to the octahedral tilts. This is shown in the model in Figure 6c (right). A new cross section TEM sample was then prepared oriented at 45° from the first one and the obtained HRTEM image is shown in Figure 6(b). The two contrast modulations are observed, corresponding to the octahedral and square plane columns oriented out of plane as expected from the structural model.

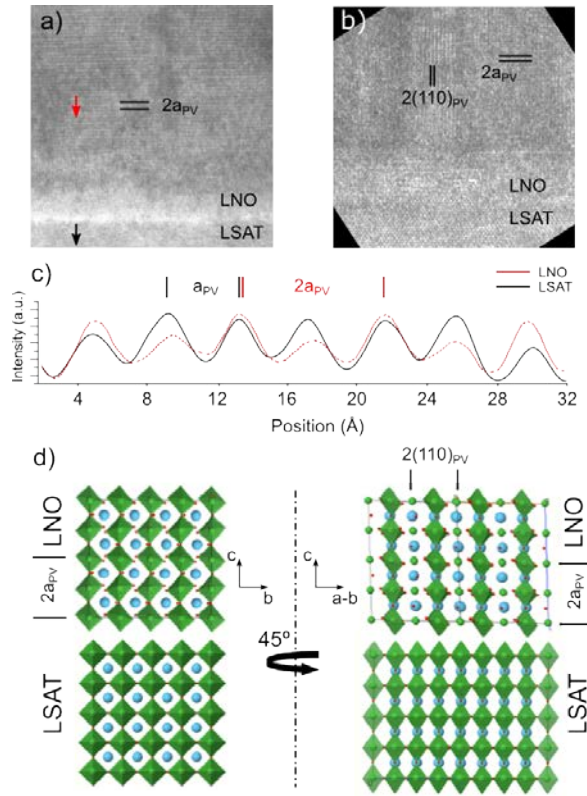


Fig. 6. a) HRTEM image of the 35 nm LNO film on LSAT observed along the [100] direction. b) HRTEM image of the same film, from a TEM specimen prepared at 45° from the one in (a), thus observed along the [110] direction. Superstructure contrast modulation is faint but visible in both orientations. c) Intensity profiles taken in the substrate (black) and superstructure region in LNO (red), as indicated by arrows in panel a), showing the double periodicity. d) Structural model of the $\text{LaNiO}_{2.5}$ /LSAT interface showing the origin of the modulations in (a) and (b): the effect of alternating columns of octahedral and planar columns is superimposed to that of the octahedral tilt pattern.

In summary, the observed superstructure modulation in LNO thin films is found to be compatible with a lower symmetry, oxygen deficient, monoclinic $\text{LaNiO}_{2.5}$ phase. The octahedral tilt induced by the oxygen vacancies is observed in different orientations depending on the sign of the stress exerted by the substrate. This is related to the in-plane or out-of-plane orientation of the shorter monoclinic c axis. By choosing an adequate geometry for the TEM specimen preparation in each case, the crystal orientations revealing the alternating octahedral and planar square coordinated columns can be accessed.

Regarding the 14 nm films, no superstructure modulation is observed. A first explanation for the absence of visible modulation is that no oxygen vacancies exist in the thinner films. However, at first sight, using the same arguments concerning the thermodynamic instability of Ni^{3+} , the subsequent presence of oxygen vacancies may still hold. However, in the energy balance involved in the thermodynamic equilibrium, the elastic energy associated to the epitaxial strain should be included and this increases with film thickness. Therefore, it may well occur that for the 14 nm, the epitaxial strain is simply stored in the form of elastic energy whereas at larger thickness, the exceedingly large elastic energy is partially released by introduction of oxygen vacancies which, eventually, order as in $\text{LaNiO}_{2.5}$. In a second scenario, oxygen vacancies could exist also in the 14 nm films but their concentration not high enough to promote order and thus they are invisible in the HRTEM images. It is worth pointing out the importance of stoichiometry as a strain relaxation mechanism in complex oxides, especially as films grow thicker.

Interestingly, the macroscopically measured conductivity values show a metallic behaviour for all the films [Weber2016]. However, all known oxygen deficient phases ($\text{LaNiO}_{3-\delta}$) are reported to be insulating [Sanchez1996], consistently with the necessary octahedral connectivity for orbital hybridization. This apparent contradiction can be understood considering that the detected oxygen deficient phase is a minor fraction of the 35 nm films and does not break the percolation of metallic regions; in the 14 nm films, oxygen vacancies, if any, are randomly distributed, and thus the films are also metallic. Besides explaining the metallic behaviour observed in our films, these results further emphasize the importance of strain engineering in the control of transport properties of rare earth nickelates. The effect of lattice parameter mismatch with respect

to the substrate, but also film thickness and oxygen atmosphere conditions on the strain state and stoichiometry of the films offer a wide range of possibilities for the fine tuning of transport properties.

6. Summary and conclusions

14 and 35 nm thick LNO films grown on LAO and LSAT substrates have been characterized to study the different epitaxial strain states induced in the LNO films by the crystal lattice mismatch with each substrate. A good epitaxial growth of the films is confirmed from HRTEM and HAADF experiments. LNO films on LAO and LSAT are found to be completely adapted to the substrate. The strain state of the LNO films has been studied by GPA. The results show fully strained LNO films in the in-plane direction and values close to those of bulk LNO for the out-of-plane parameter.

A local superstructure modulation has been observed in the 35 nm LNO films grown on LAO and LSAT, which has been found to correspond to $\text{LaNiO}_{2.5}$, a monoclinic oxygen deficient phase. The difference in the sign of the strain exerted by the LAO and LSAT substrates is found to lead to two different orientations of the monoclinic axes of $\text{LaNiO}_{2.5}$. Through an adequate TEM specimen preparation process, different zone axes of the oxygen deficient phase have been made accessible for observation.

Both the strain exerted by the substrate, that affects the Ni-O angles and distances and, therefore, the orbital hybridization, and the non-stoichiometry of the films, that affects the octahedral network connectivity, are major aspects affecting the electrical transport properties of LNO.

ACKNOWLEDGEMENTS

LLC, JMR, SE and FP acknowledge financial support by the Spanish Government (projects MAT2013-41506 and CSD2009-2013). ICMAB activity has been sponsored by the Spanish MINECO (Project:MAT2014-56063-C02) and the “Severo Ochoa” Programme for Centres of Excellence in R&D (SEV-2015-0496)), and by Generalitat de Catalunya (2014 SGR 00734). TEM facilities at CCiT-UB, CEMES-CNRS and LMA-INA are also acknowledged.

REFERENCES

- [**Xu1993**] X.Q. Xu, J.L. Peng, Y. Li, H.L. Ju, and R.L. Greene. Resistivity, thermopower, and susceptibility of RNiO_3 ($R = \text{La, Pr}$). *Phys. Rev. B Condens. Matter* 48(2):1112–1118, 1993.
- [**Zhu2013**] M. Zhu, P. Komissinskiy, A. Radetinac, M. Vafaei, Z. Wang, and L. Alf. Effect of composition and strain on the electrical properties of LaNiO_3 thin films. *Applied Physics Letters*, 103(14):141902, 2013.
- [**Scherwitzl2009**] R. Scherwitzl, P. Zubko, C. Lichtensteiger, and J.M. Triscone. Electric-field tuning of the metal-insulator transition in ultrathin films of LaNiO_3 . *Applied Physics Letters*, 95(22):222114, 2009.
- [**Poltavets2010**] V.V. Poltavets, K.A. Lokshin, A.H. Nevidomskyy, M. Croft, T.A. Tyson, J. Hadermann, G. Van Tendeloo, T. Egami, G. Kotliar, N. ApRoberts-Warren, A.P. Dioguardi, N.J. Curro and Martha Greenblatt. Bulk Magnetic Order in a Two-Dimensional $\text{Ni}^{1+}/\text{Ni}^{2+}$ (d^9/d^8) Nickelate, Isoelectronic with Superconducting Cuprates
- [**Weber2016**] M. C. Weber, M. Guennou, N. Dix, D. Pesquera, F. Sánchez, G. Herranz, J. Fontcuberta, L. López-Conesa, S. Estradé, F. Peiró, Jorge Iñiguez and J. Kreisel. Multiple strain-induced phase transitions in LaNiO_3 thin films. *Phys. Rev. B* 94, 014118, 2016
- [**Coll2016**] C. Coll, L. López-Conesa, J. M. Rebled, C. Magén, F. Sánchez, J. Fontcuberta, S. Estradé, F. Peiró. Simulation of STEM-HAADF image contrast of Ruddlesden-Popper faulted LaNiO_3 thin films (submitted)
- [**Alonso1997**] J.A. Alonso, M.J. Martínez-Lope, J.L. García-Muñoz, and M.T. Fernández-Díaz. A structural and magnetic study of the defect perovskite $\text{LaNiO}_{2.5}$ from high-resolution neutron diffraction data. *J. Phys. Condens. Matter*, 6417–6426, 1997.
- [**Kinyanjui2014**] M.K. Kinyanjui, Y. Lu, N. Gauquelin, M. Wu, A. Frano, P. Wochner, M. Reehuis, G. Christiani, G. Logvenov, H.U. Habermeier, G.A. Botton, U. Kaiser, B. Keimer, and E. Benckiser. Lattice distortions and octahedral rotations in epitaxially strained $\text{LaNiO}_3/\text{LaAlO}_3$ superlattices. *Applied Physics Letters*, 104(22):221909, 2014.
- [**Hwang2013**] J. Hwang, J. Son, J Zhang, A. Janotti, C. Van de Walle, and S. Stemmer. Structural origins of the properties of rare earth nickelate superlattices. *Physical Review B*, 87(6):060101, 2013.
- [**Sakai2013**] E. Sakai, M. Tamamitsu, K. Yoshimatsu, S. Okamoto, K. Horiba, M. Oshima, and H. Kumigashira. Gradual localization of Ni 3d states in LaNiO_3 ultrathin films induced by dimension. *Physical Review B*, 87(7):075132, 2013.
- [**Snoeck1998**] M.J. Hÿtch, E. Snoeck, and R. Kilaas. Quantitative measurement of displacement and strain fields from HREM micrographs. *Ultramicroscopy*, 74(3):131–146, 1998.
- [**Woodward2005**] D.I. Woodward and I.M. Reaney. Electron diffraction of tilted

perovskites. *Acta crystallographica. Section B, Structural science*, 61(4):387–99, 2005.

[**Stolen2005**] S. Stølen, C.E. Mohn, P. Ravindran, and N.L. Allan. Topography of the potential energy hypersurface and criteria for fast-ion conduction in perovskite-related $A_2B_2O_5$ oxides. *The journal of physical chemistry. B*, 109(25):12362–5, 2005.

[**Stolen2006**] S. Stølen, E. Bakken, and C.E. Mohn. Oxygen-deficient perovskites: linking structure, energetics and ion transport. *Physical chemistry chemical physics: PCCP*, 8(4):429–47, 2006.

[**Crespin1983**] M. Crespin, P. Levitz, and L. Gataineau. *J. Chem. Soc. Faraday Trans.*, 1983.

[**GonCal1989**] J.M. González-Calbet, M.J. Sayagués, and M. Vallet-Regi. An electron diffraction study of new phases in the $LaNiO_{3-x}$ system. 1989, *Solid State Ionics*.

[**Moriga1994**] T. Moriga, O. Usaka, T. Inamura, I. Nakabayashi, I. Matsubara, T. Kinouchi, S. Kikkawa, and F. Kanamaru. *Bull. Chem. Soc. Japan*, 1994.

[**Alonso1995**] J.A. Alonso and M.J. Martínez-Lope. Preparation and crystal structure of the deficient perovskite $LaNiO_{2.5}$, solved from neutron powder diffraction data. *Journal of the Chemical Society, Dalton Transactions*, (17):2819, 1995.

[**Sanchez1996**] R.D. Sánchez, M.T. Causa, A. Caneiro, A. Butera, M. Vallet-Regi, M.J. Sayagués, J. González-Calbet, F. García-Sanz and J. Rivas. Metal-insulator transition in oxygen deficient $LaNiO_{3-\delta}$ perovskites, *Physical Review B* 54(23), 1996